

Acoustoelectric drag current in vanadium oxide films

Cite as: J. Appl. Phys. **128**, 155104 (2020); <https://doi.org/10.1063/5.0015215>

Submitted: 26 May 2020 . Accepted: 26 September 2020 . Published Online: 16 October 2020

Pavel N. Lapa , George Kassabian, Felipe Torres, Pavel Salev, Min-Han Lee , Javier del Valle, and Ivan K. Schuller



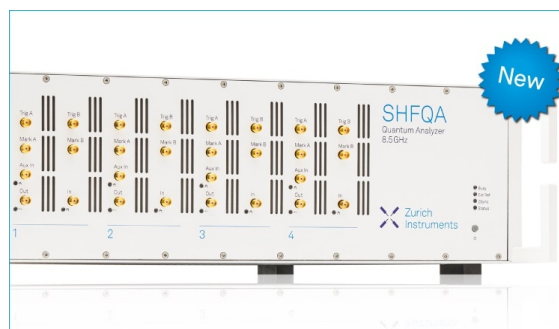
View Online



Export Citation



CrossMark



Your Qubits. Measured.

Meet the next generation of quantum analyzers

- Readout for up to 64 qubits
- Operation at up to 8.5 GHz, mixer-calibration-free
- Signal optimization with minimal latency

Find out more





Acoustoelectric drag current in vanadium oxide films

Cite as: J. Appl. Phys. 128, 155104 (2020); doi: 10.1063/5.0015215

Submitted: 26 May 2020 · Accepted: 26 September 2020 ·

Published Online: 16 October 2020



Pavel N. Lapa,^{1,a)}  George Kassabian,¹ Felipe Torres,^{2,3} Pavel Salev,¹ Min-Han Lee,¹  Javier del Valle,¹ and Ivan K. Schuller¹

AFFILIATIONS

¹Department of Physics, University of California, San Diego, La Jolla, California 92093, USA

²Department of Physics, University of Chile, Santiago 7800024, Chile

³Center for the Development of Nanoscience and Nanotechnology, Estación Central, Santiago 9170124, Chile

^{a)}Author to whom correspondence should be addressed: plapa@physics.ucsd.edu

ABSTRACT

Two different Mott insulator wires, vanadium dioxide and vanadium sesquioxide, were prepared on the piezoelectric LiNbO₃ substrates. Coupling of acoustic waves propagating in LiNbO₃ with free carriers in vanadium oxide gives rise to the acoustoelectric effect that manifests itself as the generation of direct electric current by the acoustic wave. According to a phenomenological model, the value of the effect strongly depends on the wires conductivity, which, for the vanadium-oxide films, changes by a few orders of magnitude. We demonstrated that this yields a significant enhancement of the direct current (DC) current generated in the wires at the metal-insulator transition temperatures. The sign of the generated DC voltage is different for excitations by surface and bulk acoustic wave modes, which may happen due to reverse wave propagation at the substrate surface. For each resonance mode, polarities of the generated DC signal are the same in both wires, despite the signs of charge carriers being different for these materials. It was shown that two complementary techniques (acoustoelectric and Hall effect measurements) yield opposite signs of charge carriers in VO₂.

Published under license by AIP Publishing. <https://doi.org/10.1063/5.0015215>

I. INTRODUCTION

Mutually coupled mechanical and electric excitations emerging in piezoelectric heterostructures give rise to unique interaction mechanisms between the acoustic waves and charge carriers. First, the interaction of charge carriers with the potential wells created by the acoustic and electric excitations leads to acoustic waves attenuation.^{1,2} The sign of the attenuation coefficient becomes negative if the carriers' drift velocity exceeds the sound velocity, which causes amplification of an acoustic wave if sufficiently high electric current flows through a piezoelectric crystal^{3,4} or a thin film on a piezoelectric substrate.⁵ Second, due to the attenuation, the acoustic wave is constantly slowing down during its propagation. Hence, the flux of momentum associated with the acoustic wave motion is transferred to the internal degrees of freedom, including the motion of free charge carriers. This leads to induction of a direct current (DC) along the propagation direction of the acoustic wave. The phenomenon is called acoustoelectric effect (AE) or AE drag effect, while the induced DC current is usually referred as an AE current. Similarly to the Hall effect, the sign of the AE current is defined by

the type of carriers. If the positive direction is chosen along the acoustic wave vector, flow of the carrier creates a positive AE current when the majority of the carriers are holes and a negative current in the case of electron transport.

Vanadium dioxide (VO₂) and sesquioxide (V₂O₃) films undergo metal-insulator (MI) transition, which results in a significant modification of their electronic and crystallographic structures.^{6–9} This peculiar tunability is actively exploited for developing vanadium-oxide-based switchable devices,^{10,11} as well as thermally and mechanically reconfigurable electronic elements.¹² We were motivated to study the AE effect in these vanadium oxides for two main reasons. First, according to the phenomenological theory, dissipation of an acoustic wave in the materials, and hence the induced AE current, strongly depend on the material's electric (mobility of carriers and conductivity) and mechanical properties. It is expected that the substantial modification of the parameters strongly influences the AE current at the MI temperature, T_{MI} . Second, the fraction and spatial distribution of metallic and insulating phases, coexisting at temperatures around T_{MI} , may be significantly tuned by applying an external pressure.¹² Contraction and

expansion produced by an acoustic wave may drastically modify the mechanical and electronic properties of the vanadium oxides at the microscopic scale.¹³ Under certain conditions, an acoustic wave may produce a conductivity wave in the VO_2 and V_2O_3 wires. Electron scattering on the propagating areas with high and low conductivity may significantly enhanced the AE current at the MI transition.

II. EXPERIMENTAL DETAILS

70-nm thick VO_2 and V_2O_3 films were grown by rf magnetron sputtering from the V_2O_3 target on 128° Y-X cut LiNbO_3 substrates. The dimensions of the substrates are $28 \times 21 \times 0.5 \text{ mm}^3$. V_2O_3 films were sputtered at 650°C and rapidly quenched in 7.7-mTorr high-purity argon environment.¹⁴ VO_2 films were sputtered at 520°C and cooled down ($50^\circ\text{C}/\text{min}$) in a 4-mTorr gas mixture containing high-purity argon (92%) and oxygen (8%). $2.5 \text{ mm} \times 100 \mu\text{m}$ VO_2 and V_2O_3 wires were fabricated by reactive ion etching in Ar/Cl_2 . In order to excite acoustic waves, an interdigital transducer (IDT) was defined in the middle of the substrates [Fig. 1(a)]. The IDT consists of 25 pairs of $80\text{-}\mu\text{m}$ electrodes;

the distance between the electrodes is $80 \mu\text{m}$. The acoustic aperture of the IDT is 9.5 mm ; excited acoustic waves travel along the crystallographic x-direction of LiNbO_3 . While making the IDT, a series of contact patches were formed at the end on vanadium-oxide wires for wire-bonding [Fig. 1(a)]. The composition of IDT and contact patches is Ta(5 nm)/Pt (50 nm).

All the presented data were obtained using the devices with a single IDT in the middle of the substrates. For typically used devices with two IDTs, multiple reflection from a receiver may appear, resulting in strong standing waves; the produced distortion may reduce the AE effect and make analysis of the data more complicated. However, certain measurements were repeated later for a sample with two IDTs, and the observed phenomena are almost identical to those obtained for the single IDT devices. To suppress the acoustic waves reflected from the edge of the samples, a rubber-cement absorber was placed on the substrates' surfaces close to their edges [Fig. 1(a)].

Excitation of the IDTs was produced using a Tektronix AFG3252C generator, while a response of the IDTs on certain frequency is acquired by connecting a Tektronix TDS3014 oscilloscope into the generation circuit through an inductive coupler [Fig. 1(a)]. Open and short circuitries were used to study the DC response of the wires. In the case of the short-circuit measurements, the wires were connected directly to a 6517B Keithley electrometer and the DC short-circuit current was measured, while for the open-circuit measurements, the wires were connected to 2182A Keithley nanovoltmeter and the DC voltage was measured. Resistance measurements were conducted using a 6620 Keithley current source and the nanovoltmeter. Time dependences of the AE voltage were obtained using the oscilloscope in combination with a SR650 preamplifier. The dependence of the AE voltage on excitation power was acquired by modulating the amplitude of the IDT excitation and measuring modulated AE voltage using the SR650 preamplifier and a SR830 lock-in amplifier. The Hall effect measurements were conducted using $2 \text{ mm} \times 100 \mu\text{m}$ VO_2 and V_2O_3 Hall bars [inset in Fig. 3(a)] with Ti/Au contact patches. The time dependences of resistance (Fig. S1 in the [supplementary material](#)) were obtained using an electronic bridge operated with low-power amplitude modulated voltage. This sensitive lock-in technique enables detecting a small change in resistance with very high accuracy while minimizing undesirable heating of the wire by the measuring current. The samples were installed in a liquid nitrogen gas-flow cryostat where temperature was varied in the $80\text{--}380 \text{ K}$ range. COMSOL Multiphysics was used for the finite-element simulations.

III. EXPERIMENTAL RESULTS

The temperature dependences of resistivity for the V_2O_3 (left, black curve) and VO_2 (right, red curve) wires grown on the 128° Y-X cut LiNbO_3 substrates are shown in Fig. 1. V_2O_3 and VO_2 demonstrate the MI transitions at around 141 and 341 K, respectively. V_2O_3 exhibits metallic behavior above T_{MI} : its resistivity decreases with decreasing temperature. At the MI transition, the resistivity increases by about 5 orders of magnitude, which is followed by a semiconducting rise at lower temperatures. Resistivity of the VO_2 wire increases with decreasing temperature above and below transition. At T_{MI} , resistivity of the VO_2 wire sharply changes by 2.5 orders of magnitude.

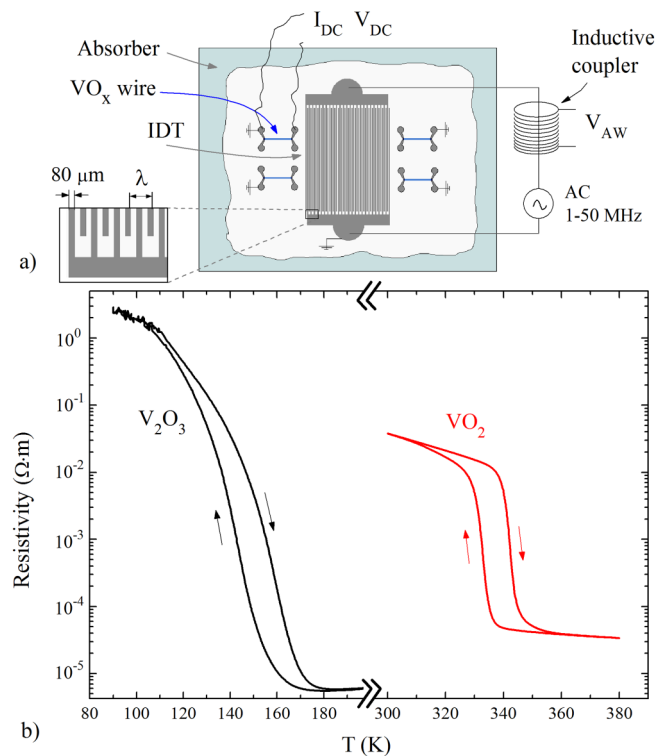


FIG. 1. (a) Schematics of the samples [a vanadium-oxide wire, an interdigital transducer (IDT), and an acoustic-wave absorber]. The size of the sample is $28 \times 21 \times 0.5 \text{ mm}^3$. The schematics demonstrates the measured parameters: DC current and voltage (I_{DC} , V_{DC}) on the wire and V_{AW} on the inductive coupler. The magnified portion of the IDT shows the comb structure with $80\text{-}\mu\text{m}$ electrodes. (b) Temperature dependences of resistivity for the V_2O_3 (left, black curve) and VO_2 (right, red curve) wires grown on the 128° Y-X cut LiNbO_3 substrates.

To study the AE effect in the V_2O_3 and VO_2 wires, frequency of an AC signal applied to the IDT was swept between 1 and 50 MHz while measuring three parameters: amplitude of an AC current on the inductive coupler (V_{AW}), DC current (I_{DC}), and DC voltage (V_{DC}) in the wires. Figure 2 shows spectra obtained for the V_2O_3 wire (black line) and VO_2 wire (red line) devices at around T_{MI} (141 K and 341 K), respectively. The spectra were obtained with a fixed amplitude of the RF signal applied to the IDT; peak-to-peak voltage is 5 V, which corresponds to 18 dBm of the RF power. The spectra at different temperatures look qualitatively similar, and only the absolute magnitudes of the peaks change. The relative amplitude and the shape of the curves remain about the same. At certain frequencies, the AC field applied to IDT causes resonance excitation of acoustic waves. The change in the IDT-circuit impedance results in pronounced peaks of V_{AW} [Fig. 2(a)]. Thus, the frequency dependence of V_{AW} conveys the spectral characteristic of an acoustic wave excited in $LiNbO_3$. The resonance at 12.25 MHz corresponds to a fundamental surface-acoustic-wave (SAW) mode. Estimation of the SAW resonance frequency, f_{SAW} , with expression v/λ , where $v = 3978$ m/s is sound velocity in 128° Y-X cut $LiNbO_3$ ¹⁵ and λ is a wavelength which is equal to $320 \mu\text{m}$ (double distance between the centers of two consecutive electrodes of the IDT), providing $f_{SAW} = 12.43$ MHz. The simulations show that the peaks observed at

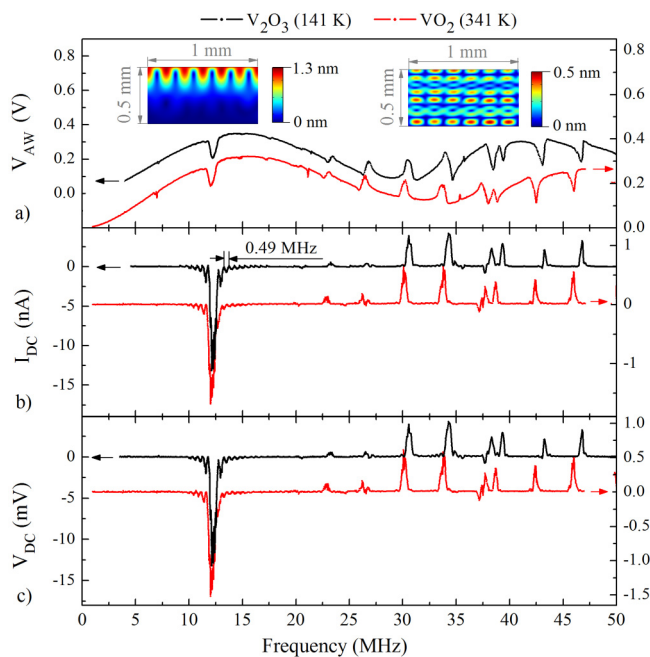


FIG. 2. (a) Voltage induced on the inductive coupler of the IDT circuit (V_{AW}), (b) DC current (I_{DC}), and (c) DC voltage (V_{DC}) induced in the vanadium-oxide wires as functions of excitation frequency. Black curves show spectra for the V_2O_3 wire at 141 K (right scale bar). Red curves show spectra for the VO_2 wire at 341 K (right scale bar). The insets in (a) depict the mechanical displacement along the wires for surface and bulk acoustic waves (12.25 and 30.2 MHz, respectively).

higher frequencies correspond to bulk acoustic wave (BAW) resonances.¹⁶ Insets in Fig. 2(a) depict the amplitude of the mechanical displacement inside the substrate caused by the 12.25-MHz SAW (the left inset) and the 30.2-MHz BAW (the right inset). The positions of the corresponding resonance peaks for the V_2O_3 and VO_2 samples are slightly different even though they have the same design of the IDT and the films were grown on the identical substrates [Fig. 2(a)]. This shift may occur because high temperature exposure affects the $LiNbO_3$ structure. Since the growth of the V_2O_3 and VO_2 films was conducted at different temperatures, the properties of the corresponding substrates get slightly different.

The DC current and voltage induced in the wires at different frequencies is shown in Figs. 2(b) and 2(c), respectively. A number of observations indicate that the DC current directly relates to the acoustic waves excited in the substrates. First, the spectra have a number of peaks, and their positions coincide with the resonant frequencies of the devices. Second, there is a series of smaller subsidiary peaks around the fundamental SAW frequency. These peaks are spaced from each other by 0.49 MHz [Fig. 2(b)], which is equal to f_{SAW}/N , where N is a number of electrode pairs in the IDTs ($N = 25$).

Polarity of the DC field induced by the acoustic waves is different for different types of excitation. I_{DC} and V_{DC} are negative for frequencies around the SAW resonance, while it is positive for the BAW resonance modes. In addition, the amplitude of I_{DC} and V_{DC} at f_{SAW} is considerably larger than that for all BAW peaks. For each excitation mode, the polarity of the DC signal induced in the V_2O_3 and VO_2 wires is the same. At the same time, the transport measurements show that VO_2 and V_2O_3 have negative and positive Hall coefficients, respectively. Figure 3(a) shows the Hall effect data in the VO_2 (red curve) and V_2O_3 (blue curve) Hall bars. The sign of the charge carrier remains the same across the transition for both materials. Thus, the Hall resistance of VO_2 is negative above and below the transition. The resistivity of V_2O_3 in the insulating phase is very high for a reliable Hall effect measurement. However, the Hall resistivity of V_2O_3 measured within the transition has the same sign (positive) as above the transition.

To investigate the change of the DC field polarity at f_{SAW} and f_{BAW} , the dependence of the DC voltage peaks on the strength of acoustic waves were studied. Figure 3(b) shows the DC voltage induced in the V_2O_3 wire at 300 K as a function of the exciting RF power at frequencies of 30.4 MHz (black dots) and 12.25 MHz (circles). A lock-in detector was used to measure induced voltage with high precision, even for low-power excitation. For this, the amplitude of the RF signal applied to the IDT was modulated at 215 Hz, while modulated DC voltage on the wire was preamplified and its amplitude was measured with lock-in detector. Figure 3(b) shows that the amplitudes of DC voltage induced by 30.4-MHz and 12.25-MHz excitation depend linearly on the acoustic wave intensity. For each peak, the DC field does not change sign in the entire studied power range.

The temperature dependences of the DC voltage, V_{DC} , and current, I_{DC} , induced by the 12.25-MHz-SAW and the 30.2-MHz-BAW excitations (18 dBm) were measured for the V_2O_3 wire [Figs. 4(a) and 4(b)] and VO_2 wire [Figs. 4(c) and 4(d)]. The DC fields induced by the BAW (data at the upper half-plane of each plot) and SAW (data at the bottom half-plane of each plot)

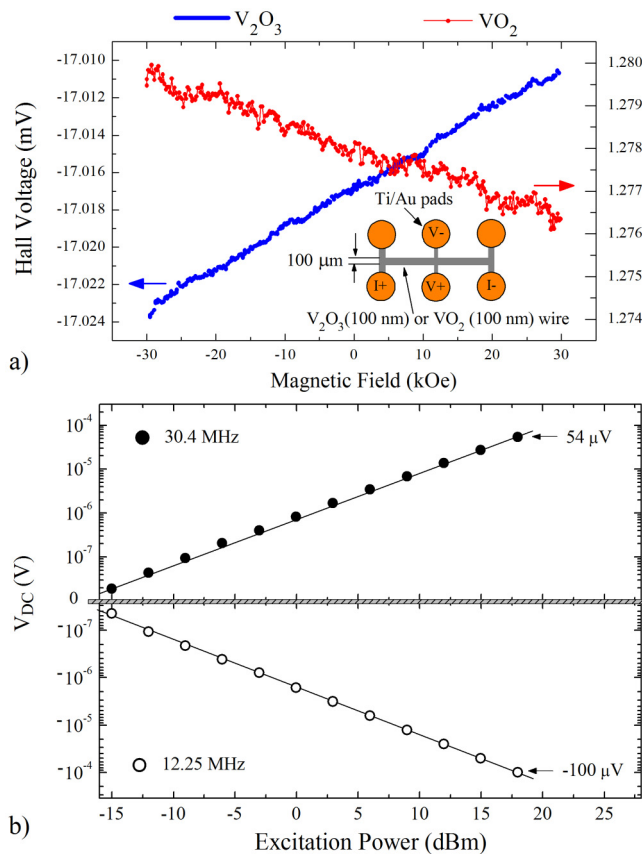


FIG. 3. (a) Magnetic field dependence of the Hall voltage at 300 K in the V_2O_3 (100 nm) (blue line) and VO_2 (100 nm) (red dots) Hall bars (inset) on the 128° Y-X cut $LiNbO_3$ substrates. (b) DC voltage, V_{DC} , induced in the V_2O_3 wire as a function of IDT excitation power with 30.4-MHz (black dots) and 12.25-MHz (circles) excitations measured at 300 K. V_{DC} is in logarithmic scale. V_{DC} induced by the 18-dBm excitation at 12.25 MHz and 30.4 MHz are $-100 \mu V$ and $54 \mu V$, respectively. The black curves are guides to the eye.

excitations remain positive and negative, respectively, in the entire studied temperature range. Similarly to the temperature dependences of resistance [Fig. 1(b)], the temperature dependences of the induced DC field (Fig. 4) exhibit hysteretic behavior around the MI transition. The absolute values of V_{DC} and I_{DC} change significantly at the MI transition. For the V_2O_3 wire, V_{DC} and I_{DC} induced by the SAW and the BAW have pronounced extremes at the transition, while these parameters experience step-like change for the VO_2 wire.

The AC current induced in the vanadium-oxide wires by an acoustic wave produces Joule heating. Since the acoustic wave gets attenuated, the heating and, hence, the temperature are not homogeneous over the length of the wires. Additionally, significant increase in the wire temperature may occur due to heat transfer from the IDT. Since the wire is located perpendicular to the IDT aperture, the opposite ends of the wire may be heated differently, and the gradient of temperature may lead to generation of a thermoelectric current. In order to empirically estimate the DC field

generated due to the inhomogeneous heating by acoustic waves, we prepared another V_2O_3 device similarly to the one shown in Fig. 1(b), but with a microheater located closed to the end of the wire nearest to the IDT (inset in Fig. 5). The microheater has a Ta (5 nm)/Pt(50 nm) structure, its width is $40 \mu m$, the length of the bar parallel to the wire is $300 \mu m$, and the full length is 1.1 mm. The purpose of this microheater is to create the same change in the wire's temperature as that during the IDT excitation, then to measure the Seebeck current produced due to this heating, and compare this value with the DC current induced by the acoustic waves.

18-dBm excitation by the SAW (12.25 MHz) and BAW (30.4 MHz) result in a rise of the V_2O_3 wire resistance by 0.1% at 300 K [Fig. S1(a) and (b) in the supplementary material]; the rise time of resistance is about 15 s. Based on the temperature dependence of resistance for the wire, 0.1% increase in resistance at 300 K corresponds to about 100-mK rise of temperature. The same change in resistance is produced by passing an 11-mA current through the microheater [Fig. S1(c) in the supplementary material]. Figure 5 shows the initial stages of DC voltage induction in the V_2O_3 wire due to the different stimuli: 18-dBm excitations of the IDT at 12.25 and 30.4 MHz, and passing the 11-mA current through the microheater with the IDT being off. These data were obtained by preamplifying the measured signal and recording it with the oscilloscope. The Seebeck voltage caused by microheater heating of the wire is negative and has the same order of magnitude as the voltage produced by the acoustic waves at 300 K. It must be emphasized that, even though the change in average temperature across the wire is intentionally set to be the same for the acoustic-wave and microheater excitations, the distribution of temperature across the wire may be very different for these stimuli. The measurements show that the averaged 100-mK increase in the wire's temperature may be associated with temperature gradient enough to induce the negative DC voltage comparable with that observed with the acoustic wave excitation. According to Fig. 5, the DC voltage induced by the acoustic waves settles very fast: the measured rise time is below $40 \mu s$. At the same time, the thermoelectric voltage induced by the microheater demonstrates a very different trend. Similarly to the time dependence of resistance (Fig. S1 in the supplementary material), the voltage rises relatively slow (about 0.5 s) after the power is applied to the microheater.

IV. DISCUSSION

The resonant excitation of acoustic waves results in the generation of the DC field in the V_2O_3 and VO_2 wires. In the entire studied temperature and excitation-power ranges, the polarities of the DC field are different for the SAW and BAW excitations. According to the Hall effect measurement, the majority of carriers in V_2O_3 are holes. Since the ground wire is connected to the ends of the wires that are more distant from the IDT, the SAW propagating away from the IDT causes the holes to flow toward the ground wire. Thus, the negative DC field generated in the V_2O_3 wire at f_{SAW} is a direct manifestation of the acoustoelectric effect. However, it is not completely clear in this description, why the BAWs induce the positive DC field in the wire. We assume that this may happen because of a complex distribution of the acoustic excitation in

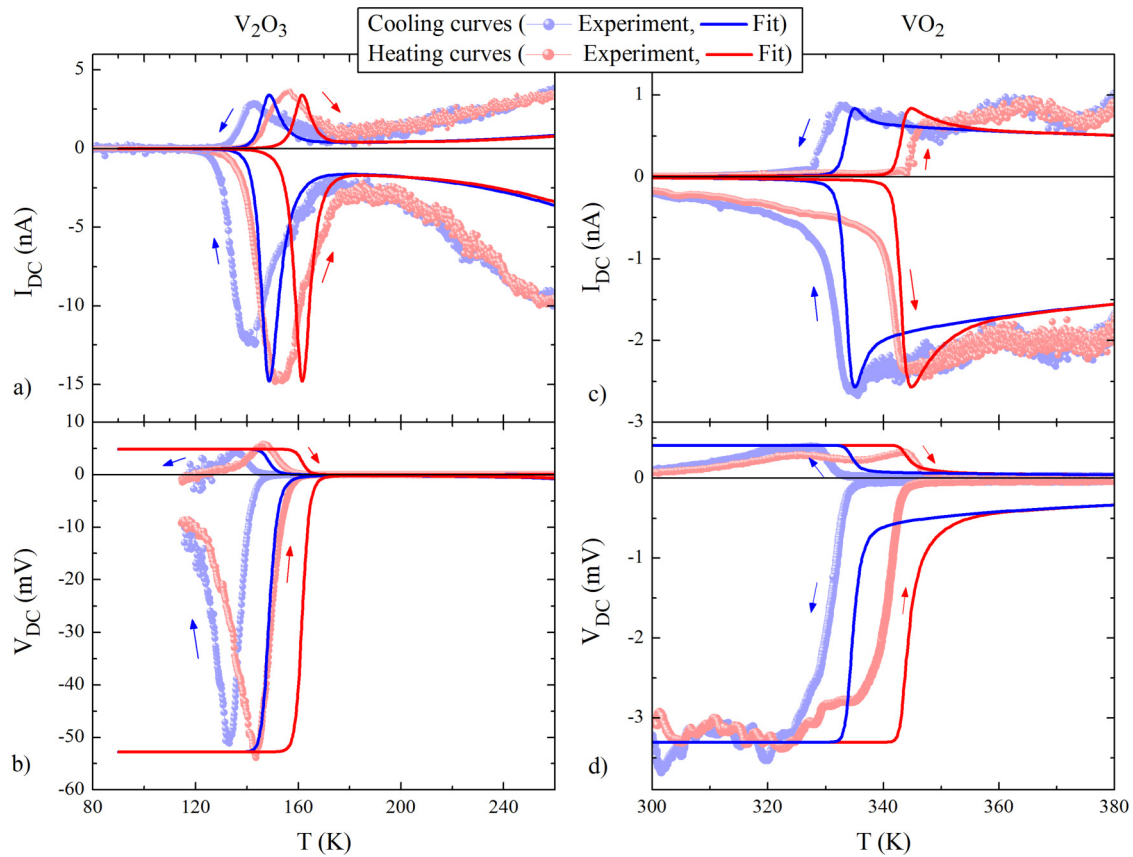


FIG. 4. Temperature dependences of DC current and voltage for the V_2O_3 [(a) and (b)] and VO_2 [(c) and (d)] wires induced by the 12.25-MHz-SAW (bottom half-plane) and the 30.2-MHz-BAW (the upper half-plane) excitations. Dotted lines show the experimental data, and thin lines are the fit to the phenomenological temperature dependences of AE current and voltage. Blue and red curves correspond to the cooling and heating branches, respectively.

$LiNbO_3$ at the BAW modes. Assumedly, a group velocity of mechanical excitation at the substrate's surface and that in the bulk of the substrate may be opposite at f_{BAW} . This backflow of acoustic wave at the surface may result in the switch of acoustoelectric field polarity at the BAW modes.

VO_2 film grown on $LiNbO_3$ has a negative Hall resistance, which is consistent with previously reported data for VO_2 films.^{17,18} This implies that the majority of carriers are electrons. In the case of the AE effect, an acoustic wave propagating away from the IDTs should cause the flow of the electrons toward the ground wire. Hence, the DC field induced by the SAW should have been positive for VO_2 , while the measured spectra have the negative peaks at f_{SAW} [Figs. 2(b) and 2(c)]. This discrepancy between the AE and Hall effect measurements of the VO_2 wire cannot be understood in the framework of the effects phenomenology. It is possible that either certain aspects of the experimental methods are inadequate for the particular material, or the phenomenon is related to a microscopic structure of VO_2 . For instance, the observed behavior may be explained if it is assumed that conductivity is not homogeneous over the VO_2 film, and the majority of carriers are opposite for high and

low conductivity areas. The Hall effect measurements are selectively sensitive to the high conductivity areas which have the electron transport. As it is clear from the phenomenological theory of the AE effect (covered below), the acoustoelectric effect is much more pronounced in the low conductivity areas where, by the assumption, the charge carriers are holes. Thus, for this particular inhomogeneity in the film, these two complimentary techniques may yield the opposite majorities of the charge carriers. We do not have any experimental results which would prove validity of the proposed model or explain why it is only applicable to VO_2 but not to V_2O_3 . The study of microscopic charge transport in VO_2 may shed light on the observed phenomena.

According to the phenomenological theory of the AE drag effect,^{19,20} the voltage across the wire of length, l , is defined as

$$V_{AE} = -\mu \frac{I\Gamma}{\sigma v} l, \quad (1)$$

where μ is mobility of charge carriers, I and v are intensity and velocity of the acoustic wave, and Γ is attenuation of an acoustic wave caused by a metallic layer with conductivity σ .²¹ For a device

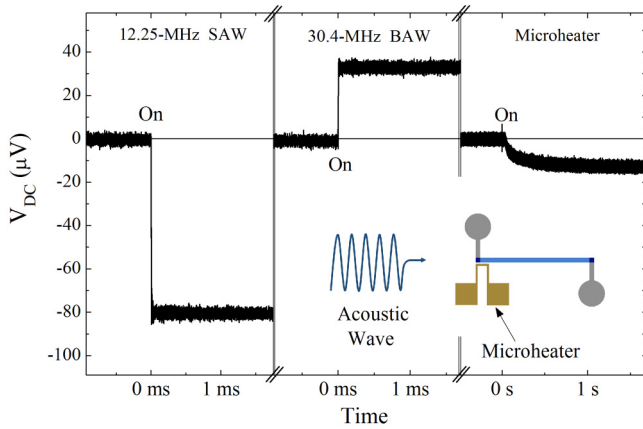


FIG. 5. Time dependence of DC voltage, V_{DC} , induced in the V_2O_3 wire due to different stimuli: 12.25-MHz SAW, 30.4-MHz BAW (18 dBm), and passing 11-mA current through the microheater. The measurements were conducted at 300 K. The inset shows the schematics of the device with the microheater. The rise time of V_{DC} induced by the acoustic waves is below 40 μ s.

composed of a non-conductive piezoelectric substrate and a conductive thin film,^{21–23} Γ is given by the expression

$$\Gamma = \pi K^2 \frac{f}{v} \left[\frac{\sigma/\sigma^*}{1 + (\sigma/\sigma^*)^2} \right], \quad (2)$$

where K^2 is the electromechanical coupling coefficient ($K^2 = 0.056$ for $LiNbO_3$), f is acoustic wave frequency. The parameter σ^* is the characteristic conductivity, which can be estimated as

$$\sigma^* = \frac{v\epsilon_0(\sqrt{\epsilon_{xx}\epsilon_{zz}} + 1)}{d} \quad \text{for SAW}, \quad (3)$$

$$\sigma^* = \frac{2\pi ft\epsilon_0(\sqrt{\epsilon_{xx}\epsilon_{zz}} + 1)}{d} \quad \text{for BAW}, \quad (4)$$

where ϵ_{xx} and ϵ_{zz} are dielectric constants of $LiNbO_3$ ($\epsilon_{xx} = 85$, $\epsilon_{zz} = 29$),²⁴ $\epsilon_0 = 8.85 \times 10^{-12}$ F/m is the permeability of free space, d and t are thicknesses of the conducting layer and the substrate, respectively. The density of the AE current in a short circuit, j_{AE} , is defined as

$$j_{AE} = \frac{V_{AE}\sigma}{l} = -\mu \frac{l\Gamma}{v}. \quad (5)$$

According to Eqs. (1)–(5), I_{DC} non-monotonically depends on the ratio of σ to σ^* . The temperature dependences of σ are different for VO_2 and V_2O_3 films (Fig. 1): for V_2O_3 , the conductivity of the metallic and insulating phases is much higher and lower, respectively, than those for VO_2 . This may explain the difference in shape of the I_{DC} - T and V_{DC} - T curves for both materials (Fig. 4). In order to estimate σ^* and compare it with the value predicted by Eqs. (3) and (4), the experimental temperature dependences of I_{DC} and V_{DC}

induced by the SAW and BAW in the V_2O_3 and VO_2 wires (Fig. 4) were fitted to the dependences expected from the phenomenological model of the AE effect, i.e., $I_{DC}(T) \sim (\sigma(T)/\sigma^*)/[1 + (\sigma(T)/\sigma^*)^2]$ and $V_{DC}(T) \sim (1/\sigma^*)/[1 + (\sigma(T)/\sigma^*)^2]$ with σ^* as a temperature-independent fitting parameter. The fit, providing the best description of the experimental curves around T_{MI} and at higher temperatures, is obtained with $\sigma^* = 10\,000 \Omega^{-1} m^{-1}$ [thin lines in Fig. 4]. This value is much higher than the characteristic conductivity expected from the phenomenological theory. Thus, according to Eqs. (3) and (4), σ^* must be 30 and $112 \Omega^{-1} m^{-1}$ for the 12.25-MHz SAW and 30.2-MHz BAW excitations, respectively. An enhanced characteristic conductivity was also reported in another work on $V_2O_3/LiNbO_3$ hybrids.²³ In that work, the attenuation of SAW by the V_2O_3 delay line was studied and it was observed that the characteristic conductivity was one order of magnitude higher than that predicted from the AE theory. The authors of that article explained this discrepancy by an assumption that, due to the percolation, the DC conductivity substituted in Eq. (2) may be significantly different from the microscopic conductivity defining the AE coupling. Additionally, it can be assumed that the conductivity of vanadium oxides may be frequency-dependent, and substitution of the DC conductivity into Eq. (2) may be an unjustified simplification. The inhomogeneous percolation in the V_2O_3 wire at low temperatures may also be responsible for the observed suppression of V_{DC} below T_{MI} [Fig. 4(b)], where the fit predicts a plateau.

The resonant excitation of acoustic waves can cause the rise of the V_2O_3 wire temperature by 100 mK at 300 K. The microheater measurements show that, in principle, this heating may result in a thermoelectric voltage comparable to the AE voltage at 300 K. However, the resistance measurements demonstrate the rise time of temperature while SAW, BAW, and microheater excitation is of the order of a few seconds (Fig. S1 in the supplementary material). At the same time, the DC field induced at f_{SAW} and f_{BAW} settles as fast as 40 μ s. It means that there is no correlation between the DC field induced at f_{SAW} and f_{BAW} and heating. Additionally, it indicates that the gradient of temperature caused by the acoustic waves is substantially smaller than the gradient produced through direct heat transfer from the microheater. Thus, the thermoelectric field caused by inhomogeneous heating of the wire by the acoustic waves is insignificant in comparison to the AE effect.

One of the motivations for this work was that, at T_{MI} of the vanadium oxides, a strain induced by the acoustic wave may affect the spatial distribution of the structural phases. This would, in turn, cause time-dependent modulation of resistivity along the wires. Scattering of electrons on the moving high-resistivity areas may result in dragging the electrons along the propagation direction of the acoustic wave. This phenomenon would manifest in the enhancement of generated DC current at T_{MI} . Although the increase in the DC field in the vicinity of the MI transition was observed for the V_2O_3 sample, it is not clear if it can be attributed to the modulation of resistivity. The phenomenological model omitting the strain-induced modification of vanadium-oxide lattice can qualitatively describe the temperature dependence of the DC field at T_{MI} . The simulations show that stress induced in the wire by the 18-dBm SAW and BAW is about 1 MPa. The estimated strain caused by the 1-MPa stress in V_2O_3 is about 3×10^{-5} .²⁵

It is possible that to achieve resistivity-wave charge transfer at T_{MB} , this stress must be significantly enhanced.^{12,26–28}

V. CONCLUSION

An acoustic wave induces the DC electric field in the VO₂ and V₂O₃ wires grown on the piezoelectric LiNbO₃ substrates. For a chosen design of the devices, the polarities of the DC field are opposite for the SAW and BAW excitations. The switch may be caused by the reverse wave propagation at the substrate surface for the BAW excitation. The polarity of the AE field induced by the SAW in the V₂O₃ wire points out that the holes are dominant charge carriers, and this result is consistent with the Hall effect measurements. Meanwhile, the AE and Hall effect measurements of the VO₂ wire yield that the majority of carriers are holes and electrons, respectively. This discrepancy is not clear. We assume that this may happen because the hole and electron transports dominate in different microscopic areas of the VO₂ wire, and the conductivity of these areas is distinctively different. When VO₂ and V₂O₃ undergo the MI transition, the AE voltage significantly changes. It was shown that this change is caused by a sharp decrease in the films conductivity at the MI transition.

SUPPLEMENTARY MATERIAL

See the [supplementary material](#) for Fig. S1 showing the change in the V₂O₃ wire resistance due to different stimuli.

ACKNOWLEDGMENTS

This research was supported by the Office of Basic Energy Science, U.S. Department of Energy (DOE), BES-DMS funded by the Department of Energy's Office of Basic Energy Science, DMR under Grant No. DE FG02 87ER-45332. F. Torres acknowledges financial support from Grant Nos. FA9550-16-1-0122, FA9550-18-1-0438, Fondecyt 1160639, and CEDENNA through the Financiamiento Basal para Centros Científicos y Tecnológicos de Excelencia-FB0807.

DATA AVAILABILITY

The data that support the findings of this study are available from the corresponding author upon reasonable request.

REFERENCES

- ¹A. R. Hutson and D. L. White, *J. Appl. Phys.* **33**, 40 (1962).
- ²K. A. Ingebrigtsen, *J. Appl. Phys.* **41**, 454 (1970).

- ³A. R. Hutson, J. H. McFee, and D. L. White, *Phys. Rev. Lett.* **7**, 237 (1961).
- ⁴J. H. Collins, K. M. Lakin, C. F. Quate, and H. J. Shaw, *Appl. Phys. Lett.* **13**, 314 (1968).
- ⁵Z. Insepov, E. Emelin, O. Kononenko, D. V. Roshchupkin, K. B. Tnyshtykbayev, and K. A. Baigarin, *Appl. Phys. Lett.* **106**, 023505 (2015).
- ⁶D. B. McWhan, T. M. Rice, and J. P. Remeika, *Phys. Rev. Lett.* **23**, 1384 (1969).
- ⁷A. Zylbersztein and N. F. Mott, *Phys. Rev. B* **11**, 4383 (1975).
- ⁸Y. Kalcheim, N. Butakov, N. M. Vargas, M.-H. Lee, J. del Valle, J. Trastoy, P. Salev, J. Schuller, and I. K. Schuller, *Phys. Rev. Lett.* **122**, 057601 (2019).
- ⁹F. J. Morin, *Phys. Rev. Lett.* **3**, 34 (1959).
- ¹⁰J. del Valle, Y. Kalcheim, J. Trastoy, A. Charnukha, D. N. Basov, and I. K. Schuller, *Phys. Rev. Appl.* **8**, 054041 (2017).
- ¹¹N. A. Butakov, M. W. Knight, T. Lewi, P. P. Iyer, D. Higgs, H. T. Chorsi, J. Trastoy, J. Del Valle Granda, I. Valmianski, C. Urban, Y. Kalcheim, P. Y. Wang, P. W. C. Hon, I. K. Schuller, and J. A. Schuller, *ACS Photonics* **5**, 4056 (2018).
- ¹²P. Salev, J. del Valle, Y. Kalcheim, and I. K. Schuller, *Proc. Natl. Acad. Sci.* **116**, 8798 (2019).
- ¹³Y. V. Ilisavskii, A. V. Goltsev, K. V. Dyakonov, N. F. Kartenko, V. V. Popov, E. Z. Yakhkind, V. P. Dyakonov, and A. V. Klimov, *JETP* **94**, 1179 (2002).
- ¹⁴J. Trastoy, Y. Kalcheim, J. del Valle, I. Valmianski, and I. K. Schuller, *J. Mater. Sci.* **53**, 9131 (2018).
- ¹⁵B. Liu, X. Chen, H. Cai, M. Mohammad Ali, X. Tian, L. Tao, Y. Yang, and T. Ren, *J. Semicond.* **37**, 021001 (2016).
- ¹⁶K.-Y. Hashimoto, *Surface Acoustic Wave Devices in Telecommunications: Modelling and Simulation* (Springer, Berlin, 2000), p. 1.
- ¹⁷T. Yamin, Y. M. Strelniker, and A. Sharoni, *Sci. Rep.* **6**, 19496 (2016).
- ¹⁸D. Ruzmetov, D. Heiman, B. B. Claffin, V. Narayanamurti, and S. Ramanathan, *Phys. Rev. B* **79**, 153107 (2009).
- ¹⁹V. I. Fal'ko, S. V. Meshkov, and S. V. Iordanskii, *Phys. Rev. B* **47**, 9910 (1993).
- ²⁰R. H. Parmenter, *Phys. Rev.* **89**, 990 (1953).
- ²¹M. Rotter, A. Wixforth, W. Ruile, D. Bernklau, and H. Riechert, *Appl. Phys. Lett.* **73**, 2128 (1998).
- ²²A. Wixforth, J. Scriba, M. Wassermeier, J. P. Kotthaus, G. Weimann, and W. Schlapp, *Phys. Rev. B* **40**, 7874 (1989).
- ²³C. Müller, A. A. Nateprov, G. Obermeier, M. Klemm, R. Tidecks, A. Wixforth, and S. Horn, *J. Appl. Phys.* **98**, 084111 (2005).
- ²⁴M. Jazbinšek and M. Zgonik, *Appl. Phys. B* **74**, 407 (2002).
- ²⁵Y. Sato and S. I. Akimoto, *J. Appl. Phys.* **50**, 5285 (1979).
- ²⁶Y. Chen, S. Zhang, F. Ke, C. Ko, S. Lee, K. Liu, B. Chen, J. W. Ager, R. Jeanloz, V. Eyert, and J. Wu, *Nano Lett.* **17**, 2512 (2017).
- ²⁷C. H. Neuman, A. W. Lawson, and R. F. Brown, *J. Chem. Phys.* **41**, 1591 (1964).
- ²⁸I. Valmianski, J. G. Ramirez, C. Urban, X. Battle, and I. K. Schuller, *Phys. Rev. B* **95**, 155132 (2017).